Materials Today Nano 22 (2023) 100334

Contents lists available at ScienceDirect

Materials Today Nano

journal homepage: https://www.evise.com/profile/#/MTNANO/login

Atomic-level insights into selective adsorption of H_2 and CO on SnO_2/CoO heterojunctions

Yunxia He [a, h], Lin Tao [b, h, **], Jing Li [a, ***], Mingjie Wu [c], Preeyaporn Poldorn [d], Davoud Dastan [e, *], Sedigheh Abbasi [f], Shuai Nie [a], Xitao Yin [g, ****], Qi Wang [a]

[a] School of Materials and Metallurgy, University of Science and Technology Liaoning, Anshan 114051, China
[b] School of Chemical Engineering, University of Science and Technology Liaoning, Anshan 114051, China
[c] Department of Chemical Engineering, McGill University, Montreal, QC H3A 0C5, Canada
[d] Department of Biochemistry, Faculty of Science, Chulalongkorn University, Bangkok 10330, Thailand
[e] Department of Materials Science and Engineering, Cornell University, Ithaca, NY 14850, USA
[f] Central Research Laboratory, Esfarayen University of Technology, Esfarayen, Iran
[g] School of Physics and Optoelectronic Engineering, Ludong University, Yantai 264000, China

ARTICLE INFO

Article history:
Received 17 November 2022
Received in revised form
14 March 2023
Accepted 31 March 2023
Available online 4 April 2023

Keywords:
First principles
Gas adsorption
Heterojunction
Selectivity
Gas sensors

ABSTRACT

Chemical resistive gas sensors prove that the interface effect of p-n heterojunction can afford a convinced gas selectivity. However, the effects of heterojunction on the sensor selectivity are still blurred and indistinct. In this study, based on the lattice mismatch theory and the adhesion function, SnO_2(100)/CoO(110) and CoO(110)/SnO_2(100) nanomaterials are structured to insight their sensing properties for H_2 and CO gases at nanoscale by first principles. The adsorption energy, adsorption distance, and the d-band center reveal the stability of H_2 and CO on the heterojunctions. Interestingly, the density of states reflects that the heterojunctions show an n-type response to CO and a p-type response to H_2. When H_2 and CO are adsorbed on CoO(110)/SnO_2(100)-O_2, there is a strong bond between CO and O_2, while the chemical bond between H_2 and O_2 is weak according to electron density. Consequently, heterojunctions have a high selectivity to CO over H_2. This work provides meaningful theoretical insight into the selective adsorption of reducing gases by heterojunctions.

1. Introduction

Recently, it has drawn lots of attention toward the fabrication of gas sensors using semiconductors [1,2], in light of the remarkable variations in their electrical resistance after subjecting to oxidizing or reducing gases [3–6]. It is easy to fabricate metal oxide nanomaterials via chemicals or vapor phase methods [7–9]. Recently, doping or surface functionalization strategy has been explored to improve metal oxides' gas-sensing selective properties [10–13]. Moreover, designing metal oxide heterojunctions as gas sensors have been proven to be one promising approach in composite-based sensors. They show new electronic and chemical features concerning the single metal oxide-based sensors [14,15]. Many studies have also demonstrated that composite metal oxides could improve gas-sensing selectivity to homogeneous gases [16–21].

A heterojunction material incorporating two components shows unique electronic effect, including band bending on Fermi level equilibration [22–27] and increased interfacial potential barrier energy [28–31]. Besides, compared with single metal oxide, it has the following characteristics. For chemical influence, heterojunctions can reduce the deactivation energy [32,33] and the presence of interfaces can synergize surface reactions [34]. For geometrical influence, the interface will directly affect the grain refinement [35] and surface activity [36], as well as the accessibility of gas on the surface [26]. The p-n heterojunction has been reported to enhance the selectivity to H_2 or CO in our previous work [18,21,37]. Unfortunately, it is still unclear enough to explain the selectivity mechanism. Therefore, it will be essential to understand the mechanism and control heterojunction's sensing behavior for future gas sensor field applications.

* Corresponding author.
** Corresponding author.
*** Corresponding author.
**** Corresponding author.
E-mail addresses: taolin@ustl.edu.cn (L. Tao), lijing_as321@163.com (J. Li), davoud.dastan@austin.utexas.edu (D. Dastan), yxtaj@163.com (X. Yin).
[h] These authors contributed equally.

https://doi.org/10.1016/j.mtnano.2023.100334
2588-8420/

Until now, among metal oxide nanomaterials semiconductors (TiO_2, ZnO_2, SnO_2, Fe_2O_3, WO_3, etc.), SnO_2 is one of the best materials to detect various gases (reducing and oxidizing). Meanwhile, SnO_2 has been extensively used in gas-sensing applications for good chemical and thermal stability and accuracy selectivity [38–43]. Accordingly, heterojunctions based on n-type metal oxide SnO_2 and other oxides have been widely studied and applied. For instance, ZnO, CuO, V_2O_5, and WO_3, coated on the SnO_2 surface to enhance gas sensing, have been studied [44–46]. In addition, many p-type metal oxides nanomaterials can be used for gas-sensing materials. CoO metal oxide, as a p-type gas-sensing material, presents several oxidation states due to the unfilled'd' electron orbital [47]. This material has an affinity with oxygen and exhibits multivalent features [48]. H_2 and CO as flammable and explosive reducing gases are widely used in reduction processes [49]. They are essential materials in industrial processes such as chemical and metallurgical production. When hydrocarbon chemical fuels are burned incompletely, the concentration ratio of H_2 and CO in the gaseous products can determine the air residual factor. Accurate determination of this ratio can significantly improve the effective utilization of chemical energy [50–54]. In addition, leakage of these dangerous gases is likely to cause safety accidents [55]. Since H_2 and CO are colorless, tasteless, odorless, and homogeneous, it is difficult to detect them [18,21,37,56]. The application of H_2 and CO coexistence field urgently needs to clarify the selectivity mechanism. Therefore, a reliable sensor with high sensitivity and selectivity for CO and H_2 is needed to ensure the safety of production, storage, and delivery. Various experiments have reported that SnO_2/Co_3O_4 heterojunctions have high selectivity for H_2 and CO [14,21,56]. However, the selective mechanism of H_2 and CO on the SnO_2/CoO is indistinct though the selectivity sensing materials to the two gases have been reported. Thus, the quantum mechanical calculation is necessary to be considered the economical and effective option to explain the selectivity phenomenon.

In this work, density functional theory was used to study the adsorption mechanism of H_2 and CO on the SnO_2/CoO. The electronic structure and bonding display different characters upon absorbing Co and H_2 on various sites of the heterojunction materials. The d-band center further explains the stability of H_2 and CO on the heterojunctions surface. We explored the transformation of electrical resistance of the heterojunctions and other properties when H_2 and CO are adsorbed on different surface sites. The increase/decrease of heterojunction resistance can indicate an n-type or p-type response to gas. It is a remarkable standard to exhibit the selectivity for H_2 and CO by the electronic resistance and transformation at the SnO_2/CoO heterojunctions. This phenomenon further provides theoretical guidance for improving the gas sensors' selectivity of H_2 and CO designation of sensing materials.

2. Methods

The Cambridge Serial Total Energy Package code [57,58] was used to accomplish all the calculations, which are based on the density functional theory [59–62]. Perdew-Burke-Ernzerh of functional was used to illustrate the electron exchange–correlation interactions [63]. Considering the system durability and speed optimization, the plane wave energies are up to 300 eV. Therefore, the wave functions were amplified for the system investigation and H_2, CO adsorption on the heterojunctions. The following calculation of H_2 and CO adsorption on the SnO_2/CoO heterojunctions was accomplished by the generalized gradient approximation. The k-points sampling of Brillouin zone grids was complemented with Monkhorst-Pack method for the bulk and the heterojunctions, respectively. When H_2 and CO adsorption on the heterojunctions with misfit dislocations, the heterojunction's geometric structure was fully relaxed until each atom reached the self-consistency convergence energy, it was set to a value of 2.0×10^{-6} eV/atom. In addition, the stress and displacement tolerance of convergence tolerance were set as 0.05 eV/Å, 0.1 GPa, and 0.002 Å, respectively. To prevent the interplays among neighboring atoms within the structure, a vacuum layer of 20 Å was chosen for every heterojunction surface material [50,64].

3. Results and discussion

3.1. Construction of heterojunctions

Based on the mismatch degree theory, SnO_2-based and CoO-based heterojunctions were established, as shown in Fig. S1 and Fig. S2. To definitive the optimal heterojunction composition structure, the adhesion work (W_{ad}) is applied to confirm the strength of the interfacial binding of SnO_2-based and CoO-based heterojunctions. W_{ad} as follows:

$$W_{ad} = \frac{E_{CoO} + E_{SnO2} - E_{SnO2/CoO}}{A} \quad (1)$$

where E_{SnO2} and E_{CoO} are the total energy of SnO_2 and CoO slab, respectively. $E_{SnO2/CoO}$ shows the total energy of the heterojunctions interface. A is the interface area. Table S1 demonstrates that the most stable CoO-based and SnO_2-based heterojunctions were determined to be the SnO_2(100)(I)/CoO(110)(II) and the CoO(110)(II)/SnO_2(100)(II), respectively. The stable heterojunctions are shown in Fig. 1.

Our previous research has suggested that gas sensors typically operate in air conditions, so oxygen's influences on the sensor must be considered [21]. Primarily, we need to determine the optimal adsorption point for oxygen molecules. For this reason, we have constructed a variety of adsorption about O_2 on SnO_2(100)(I)/CoO(110)(II) and CoO(110)(II)/SnO_2(100)(II) surfaces, which are displayed in Fig. 2. The adsorption strength of the target gas is judged by the adsorption energy (E_{ads}) and adsorption distance. The equation of E_{ads} is as follows [63,65]:

$$E_{ads} = E_{total} - E_{hetero-structure} + E_{gas} \quad (2)$$

where E_{total} shows the total energy of the entire adsorption system, $E_{hetero\text{-}structure}$ represents the heterojunctions which are the carriers of H_2 and CO, and E_{gas} represents the energy of H_2 and CO. A negative E_{ads} generally indicates that the system is energetically stable after gas adsorption [66].

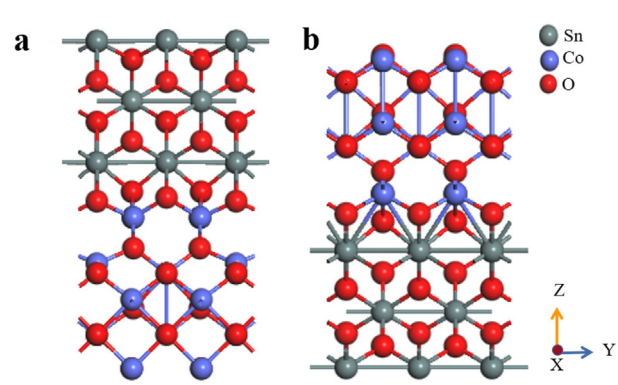

Fig. 1. Structures of the stable heterojunction. (a) SnO_2(100)(I)/CoO(110)(II) and (b) CoO(110)(II)/SnO_2(100)(II).

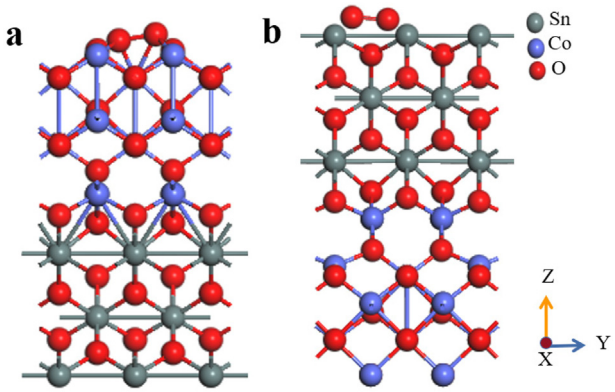

Fig. 2. The most stable adsorption structure of O_2 on heterojunctions surface. (a) O_2 on SnO2(100)(I)/CoO(110)(II) and (b) O2 on CoO(110)(II)/SnO2(100)(II).

3.2. Gas adsorption behavior on heterojunction surfaces

3.2.1. Adsorption structure of the gas–solid interface

As shown in Figs. 3 and 4, we structured five possible adsorption sites of H_2/CO on SnO_2(100)(I)/CoO(110)(II) surface and four potential adsorption sites on CoO(110)(II)/SnO_2(100)(II) surface to understand the adsorption characteristics of H_2/CO on the heterojunctions surface, respectively.

Based on the degree of lattice mismatch, the SnO_2(100) and CoO(110) facets are the best choices for constructing heterojunctions. When cutting into the crystal faces, atoms will be exposed at the crystal ends, and these end atoms will be the gas adsorption sites on the heterojunction surface. Therefore, in this study, the gas-adsorbed oxygen and exposed atoms on the surface of the heterojunctions include O_2, O1, O2, Sn of SnO_2(100)(I)/CoO(110)(II) surface, and O_2, O1, O2, Sn of CoO(110)(II)/SnO_2(100)(II) surface. The calculations of SnO_2(100)(I)/CoO(110)(II)

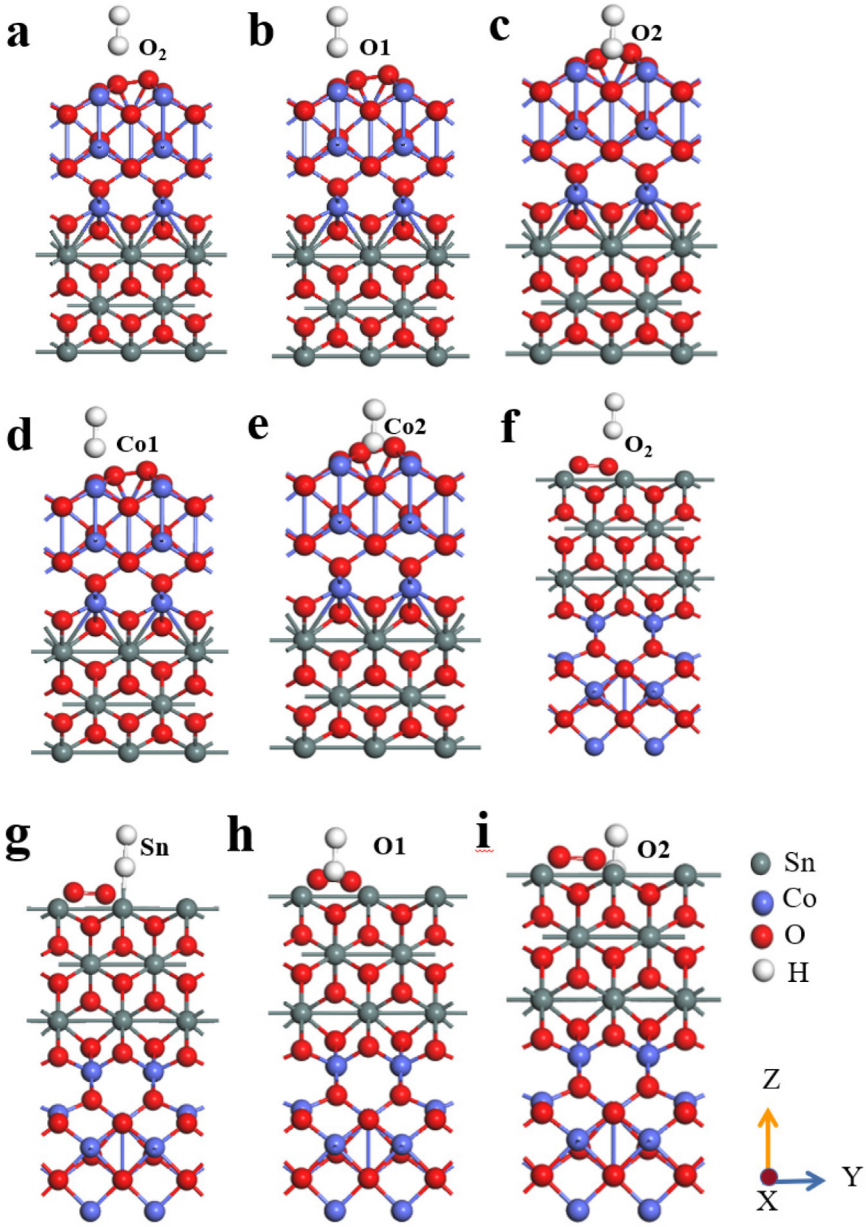

Fig. 3. H_2 is adsorbed on the heterojunction surface. (a) O_2, (b) O1, (c) O2, (d) Co1, (e) Co2 on SnO_2(100)(I)/CoO(110)(II), (f) O_2, (g) Sn, (h) O1, and (i) O2 on CoO(110)(II)/SnO_2(100)(II).

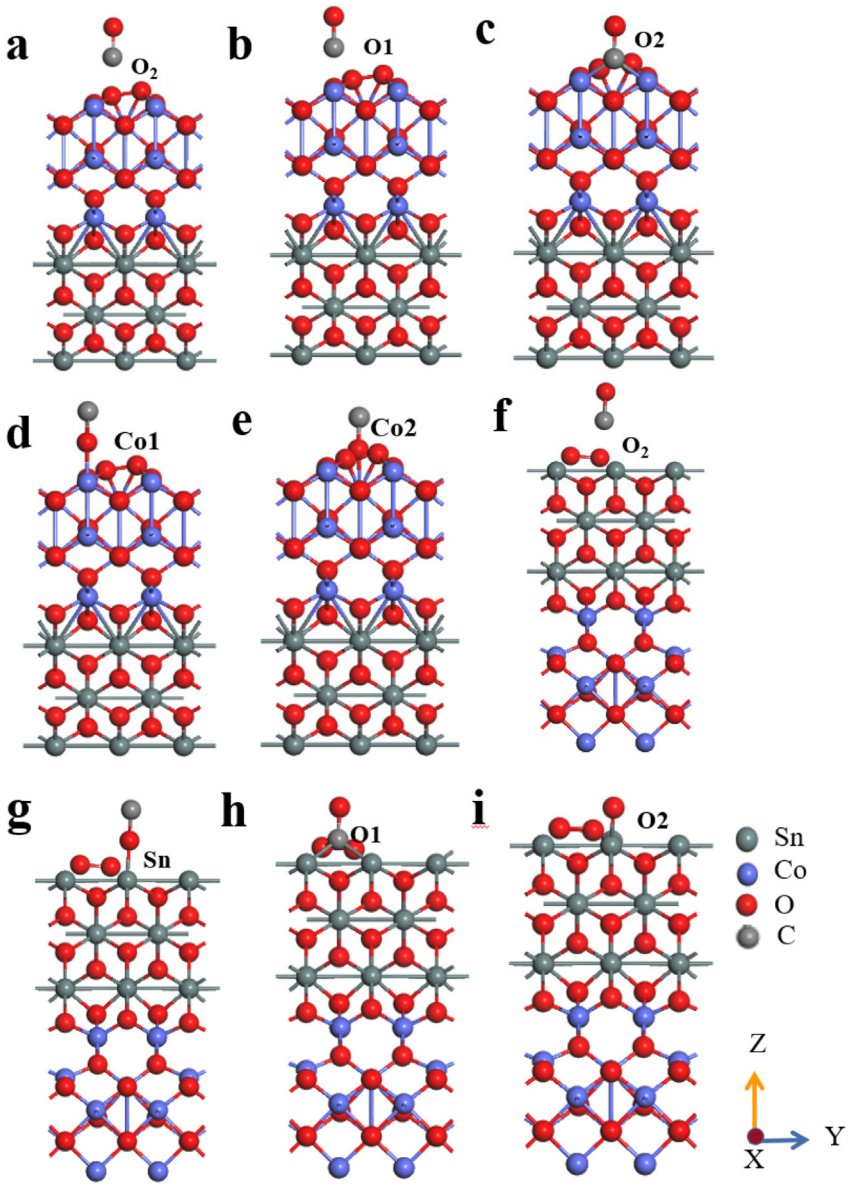

Fig. 4. CO is adsorbed on the heterojunction surface. (a) O_2, (b) O1, (c) O2, (d) Co1, (e) Co2 on SnO_2(100)(I)/CoO(110)(II), (f) O_2, (g) Sn, (h) O1, and (i) O2 on CoO(110)(II)/SnO_2(100)(II).

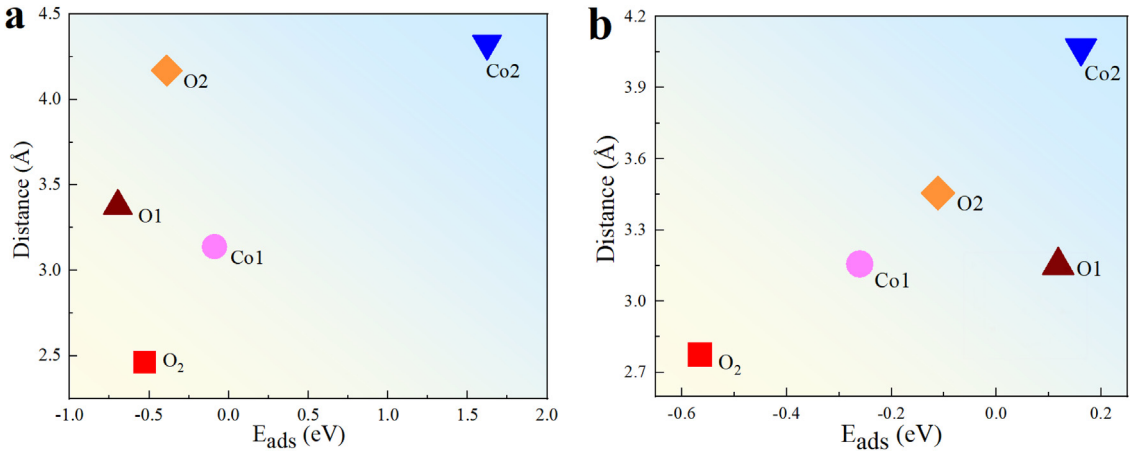

Fig. 5. Adsorption energy and distance of (a) H_2 and (b) CO on SnO_2(100)(I)/CoO(110)(II).

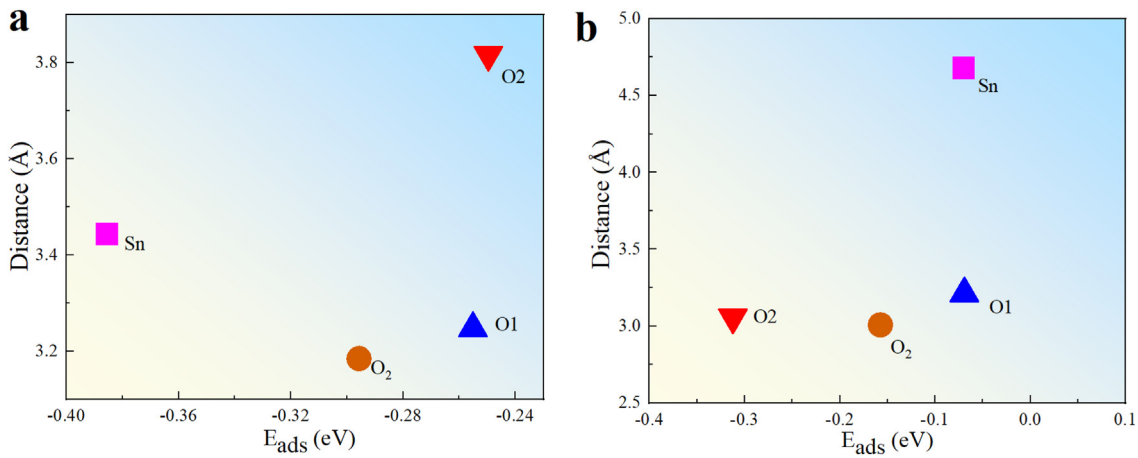

Fig. 6. Adsorption energy and distance of (a) H_2 and (b) CO on $CoO(110)(II)/SnO_2(100)(II)$.

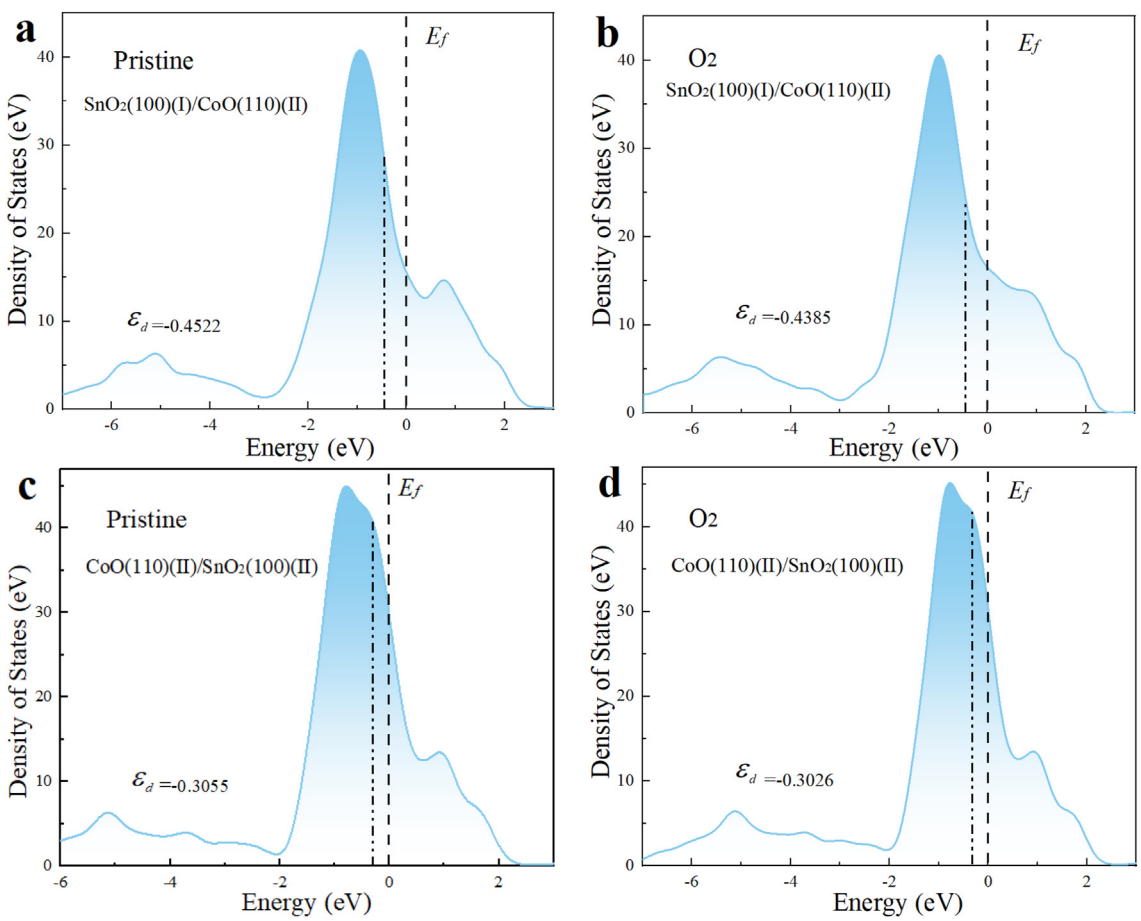

Fig. 7. The d-band center of (a) pristine and (b) O_2 of $SnO_2(100)(I)/CoO(110)(II)$, (c) pristine and (d) O_2 of $CoO(110)(II)/SnO_2(100)(II)$.

and $CoO(110)(II)/SnO_2(100)(II)$ as the carriers of H_2 and CO have been carried out successively. Moreover, all the results are summarized in Fig. 5.

As shown in Fig. 5(a), the E_{ads} of H_2 on different sites of the $SnO_2(100)(I)/CoO(110)(II)$ surface are negative, and the adsorption on CO_2 site is positive. Therefore, H_2 could be spontaneously adsorbed on the heterojunction surface beyond CO_2 site. The E_{ads} is the largest when H_2 is adsorbed on O1 site. The strongest adsorption strength means that this kind of adsorption is most likely to occur. Furthermore, the distance that H_2 is adsorbed on various sites of heterojunction surface has different degree variations than the original distance (2 Å) optimized before. However, only the adsorption distance on O_2 is smaller than 3 Å, implying the creation of chemical bonding between H_2 and O_2 molecules.

Fig. 5(b) illustrates the adsorption energy and adsorption distance of CO adsorbed on different sites of $SnO_2(100)(I)/CoO(110)(II)$ surface. The value of the adsorption energy of CO on different sites is negative, but the adsorption on CO_2 site is positive. It suggests

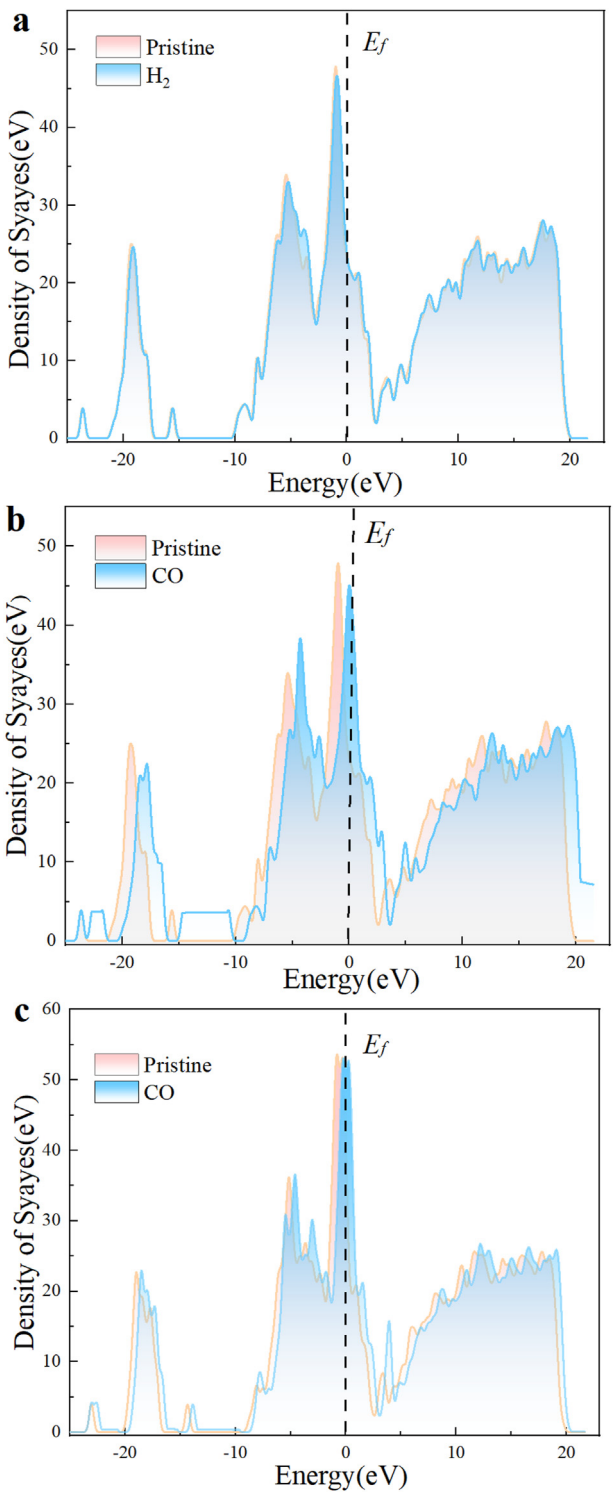

Fig. 8. DOS of (a) H_2 and (b) CO on SnO_2(100)(I)/CoO(110)(II)-O_2, (c) CO on CoO(110)(II)/SnO_2(100)(II)-O_2. DOS, density of states.

that the CO molecule could be adsorbed spontaneously on the surface of heterojunction materials outside the CO_2 site. The E_{ads} is utmost when CO is adsorbed on O2 site. It illustrates the strongest adsorption strength. In other words, this adsorption is most possible to happen. The distance that only CO on O_2 molecules of heterojunction surface is smaller than 3 Å. The existence of chemical bonding between CO and O_2 suggests that CO could be adsorbed spontaneously on the heterojunction surface.

In conclusion, the adsorption of H_2 and CO on various sites of SnO_2(100)(I)/CoO(110)(II) surface are spontaneous, outside CO_2 site. O_2 is the most stable adsorbed site for H_2 and CO. Additionally, there are bonds between O_2, H_2, and CO, respectively.

As shown in Fig. 6(a), H_2 is captured on various sites of CoO(110)(II)/SnO_2(100)(II) surface. E_{ads} is negative, and the distance is far more than 3 Å when H_2 is captured on various sites of the heterojunction materials surface. It proves that the variety adsorption is spontaneous and chemical bond does not exist. Fig. 6(b) displays the adsorption of CO on the CoO(110)(II)/SnO_2(100)(II) surface. E_{ads} is negative, and the adsorption distance is more than 3 Å, among which the adsorption distance on O_2 is close to 3 Å. Therefore, the adsorption of CO on the heterojunction surface is spontaneous. In summary, it is spontaneous adsorption when H_2 and CO are adsorbed on CoO(110)(II)/SnO_2(100)(II)-O_2, while the formation of bonds between CO and O_2 is needed further proof.

3.2.2. The d-band center

In recent years, researchers have confirmed that the d-band center can be used to reveal the changes in the adsorption energy of various surfaces adsorption when metals and their alloys are used as carriers [66,67]. Typically, a metal with active site and a higher d-band center represents potent affinity to adsorbate because of diminished filling of adsorbate-metal antibonding states. This principle has proved valuable in exploring carriers' adsorption properties in many chemical and electrochemical reactions [67–69]. The change in heterojunctions d-band center is used to predict gas adsorption capacity on the catalyst surface. Even if the adsorption energy is not calculated, the change of the d-band center will also predict the gas adsorption. Therefore, the d-band centers of pristine heterojunctions and O_2-adsorbed heterojunctions were studied to understand the adsorption of H_2 and CO. For the pristine heterojunction, Fig. 7(a) shows that the d-band center of the SnO_2(100)(I)/CoO(110)(II) is −0.4522 eV. Fig. 7(b) explains the d-band center of O_2-adsorbed heterojunction, which is close to the Fermi energy level. It illustrates that the adsorption of O_2 can significantly improve the stability of gas adsorption on SnO_2(100)(I)/CoO(110)(II) surface.

For CoO(110)(II)/SnO_2(100)(II), the d-band center of the pristine heterojunction is −0.3055 eV (Fig. 7(c)). In addition, the d-band center of O_2-adsorbed heterojunction is −0.3026 eV, closer to the Fermi energy level (Fig. 7(d)). Therefore, the adsorption of O_2 can strengthen the stability of H_2 and CO adsorption on the heterojunction surface.

3.2.3. Density of states

The adsorption of H_2 and CO impacts the heterojunction's resistance, which is reflected in density of states (DOS). Hence, the resistance changes can be studied by analyzing the DOS. The appearance of additional peaks and augmentation in the DOS amount are found in the energy ranges, which is attributed to gas adsorption. The changes in DOS are the reasons for the augmentation in electron energy and enhanced conductivity [70].

The DOS that H_2 is adsorbed on SnO_2(100)(I)/CoO(110)(II)-O_2 is shown in Fig. 8(a). The DOS value has evident decreases when H_2 is adsorbed on O_2, suggesting the slight electric resistance improvement of the heterojunction with the adsorption of H_2 on O_2. In brief, the heterojunction electrical resistance is enlarged due to the adsorption of H_2 on SnO_2(100)(I)/CoO(110)(II)-O_2. Fig. 8(b) displays the DOS about CO on SnO_2(100)(I)/CoO(110)(II)-O_2 surface. The DOS moves to the right, and the band of the system is missing among −10 to −20 eV range. The variation of DOS shows the

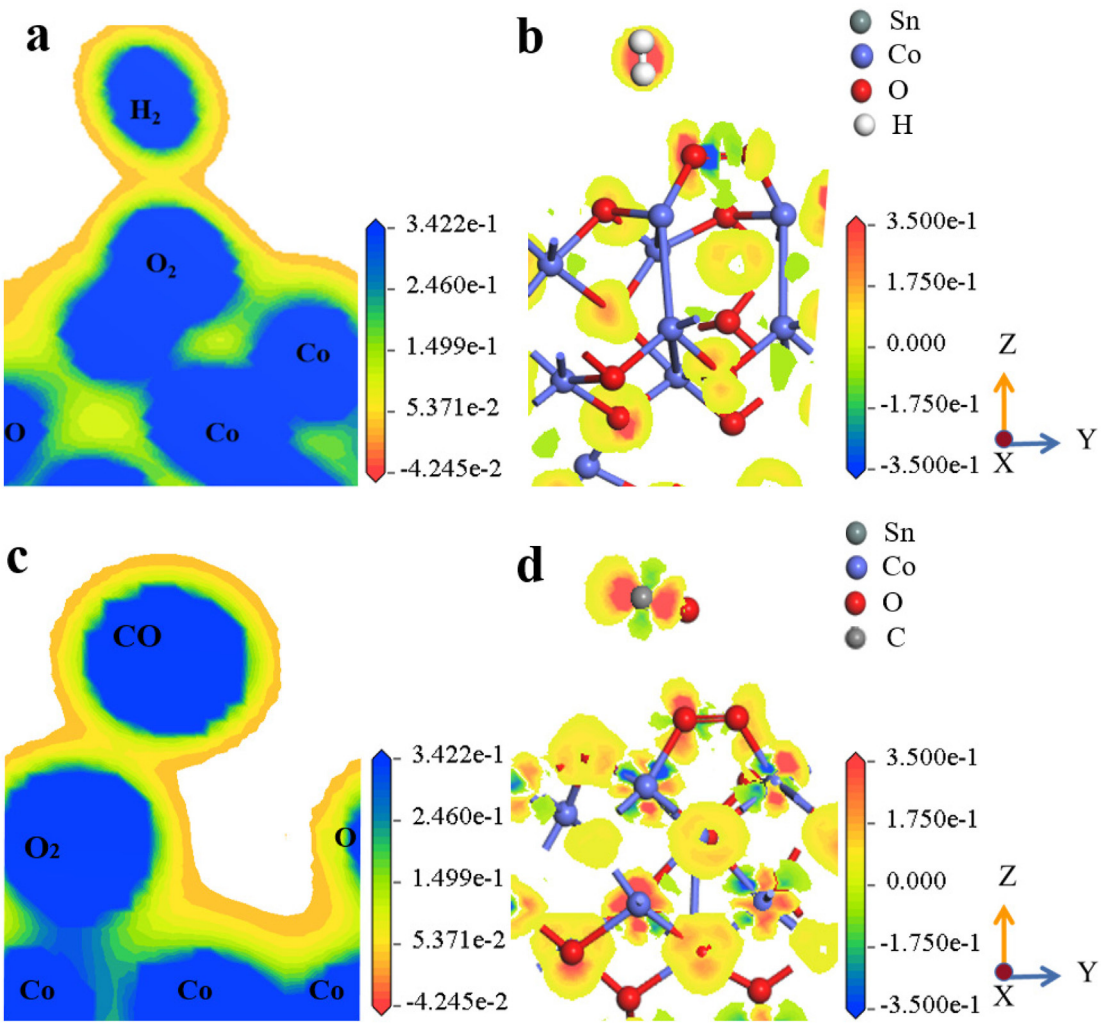

Fig. 9. (a) Electron density and (b) electron density difference of H_2 on SnO_2(100)(I)/CoO(110)(II)-O_2, (c) electron density and (d) electron density difference of CO on SnO_2(100)(I)/CoO(110)(II)-O_2.

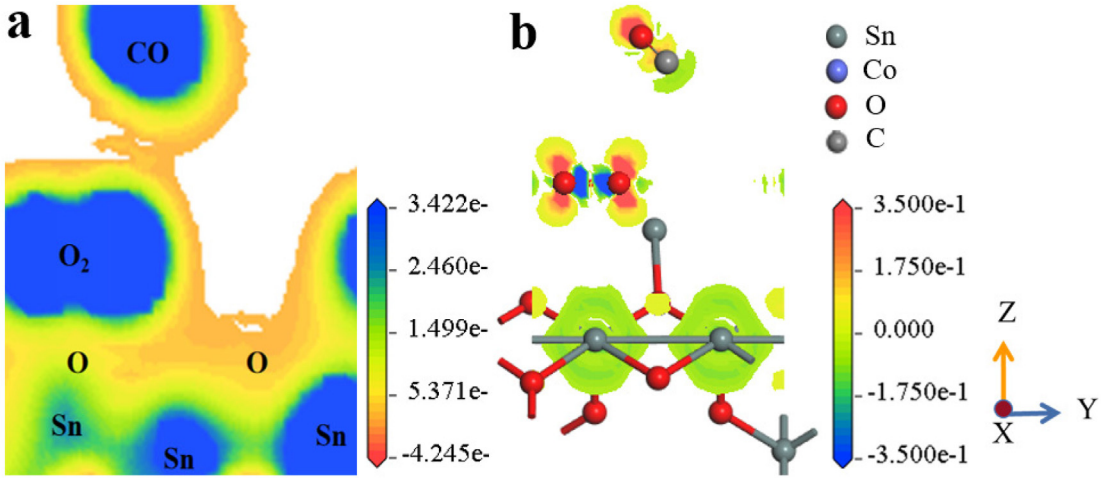

Fig. 10. (a) Electron density and (b) electron density difference of CO on CoO(110)(II)/SnO_2(100)(II)-O_2.

augmentation in electron energy and enhanced electrical conductivity. In brief, the adsorption of CO on on SnO_2(100)(I)/CoO(110)(II)-O_2 will cause smaller electrical resistance.

Fig. 8(c) shows DOS that CO is adsorbed on CoO(110)(II)/SnO_2(100)(II)-O_2. Obviously, DOS has more peaks as CO is captured on O_2-adsorbed heterojunction surface. DOS of systems are moving to the conductivity band. Changes in DOS explain better electrical conductivity. Accordingly, the electrical conductivity of CoO(110)(II)/SnO_2(100)(II) is improved when CO is captured on O_2-adsorbed heterojunction surface.

3.3. Gas–solid selectivity mechanism

3.3.1. Electronic structure of gas on SnO_2(100)(I)/CoO(110)(II)

The electronic structure and bonding could be attributed to the binding of heterojunction. The electrical density can characterize the adsorption of gases at nanoscale. To illustrate the essence of H_2 and CO adsorption on heterojunction surfaces, the electrical density and electron density difference are calculated as shown in Figs. 9 and 10.

Fig. 9 displays the electronic density and electron density difference that H_2 and CO are adsorbed on SnO_2(100)(I)/CoO(110)(II)-O_2. The blue interval exhibits the depletion zones of the electronic, and the red interval demonstrates the accumulation zone of the electronic.

As shown in Fig. 9(b), hydrogen is captured on the oxygen of the heterojunction materials surface. The electronic sharing occurs between H atoms and O_2. The adsorption distance is less than 3 Å, and E_{ads} is negative (Fig. 5(a)). Therefore, H_2 shares an appreciable electronic with O_2, indicating that –OH bonding possesses stronger covalence. In addition, O_2 can be stably adsorbed on the heterojunction surface by forming a covalent bond with the adsorption site. Because O_2 shares extensive electrons with sites on the heterojunction surface. Fig. 9(b) displays the electron density difference of H_2 on the oxygen of the heterojunction materials surface. H_2 and O_2 acquire some electrons but rarely lose electrons simultaneously. It demonstrates the appearance of electronic transmutation and chemical reactions between H_2 and O_2. The adsorption of H_2 on other sites of SnO_2(100)(I)/CoO(110)(II) surface almost does not occur, and the adsorption distance is larger than 3 Å. However, a minor electron migration between H_2 and adsorbed sites is observed, and there is no bond. As a result, O_2 has the highest adsorption site for H_2 on the heterojunction materials surface.

Fig. 9(c) illustrates the electron density that CO is adsorbed on the SnO_2(100)(I)/CoO(110)(II)-O_2. There are considerable electrons accumulated between CO and O_2. It is obvious that CO acquired ample electrons and O_2 lost some electrons. And as shown in Fig. 5(b), its adsorption distance is smaller than 3 Å and E_{ads} is negative. It proves the existence of stronger bonding and considerable electronic transformations between CO and O_2. For the CO on O_2-absorbed heterojunction surfaces (Fig. 9(d)), CO has a little change in electron acquisition and consumption, and O_2 gains numerous electrons and loses some electrons concomitantly. It reveals that there is electron transfer and reaction between them. There is a slight electron transfer between CO and other sites of the heterojunction materials surface. Summarily, the electron density of CO on the heterojunction materials surface demonstrates the existence of bond formation and electron transition. Especially, when CO is adsorbed on O_2, a stronger bond is formed between CO and adsorption sites.

3.3.2. Electronic structure of gas on CoO(110)(II)/SnO_2(100)(II)

Fig. 10 reveals the electron density difference and electron density that CO is adsorbed on CoO(110)(II)/SnO_2(100)(II)-O_2. Fig. 10(a) explains the electron density that CO is captured on oxygen of the heterojunction materials surface. Richer electrons exist between CO and O_2 on the heterojunction surface. And Fig. 6(b) explains that CO is stably adsorbed on CoO(110)(II)/SnO_2(100)(II)-O_2. It proves that there are electrical conventions and reactions between CO and O_2. Fig. 10(b) shows the electron density difference of CO on the heterojunction surface. CO obtains some electrons from O_2 on the heterojunction surface, simultaneously revealing a negligible value of electron loss. And O_2 consumes electrons and acquires some electrons at the same time. Therefore, it certificates the conversion and reaction of electrons between CO and O_2 on the heterojunction surface.

3.3.3. Gas-sensing mechanism

The electron transfer illustrates that the adsorption of CO on the heterojunctions surface is spontaneous, and there is an electron transition between CO and O_2 on the surface. And CO is more inclined to adsorb on the oxygen of the heterojunction surface. According to the above results, we have deduced the adsorption mechanism of gas on the heterojunction surface, as shown in Fig. 11.

As shown in Fig. 11, the SnO_2/CoO surface will adsorb O_2 in the air, and O_2 will be dissociated into adsorbed O (O_{ads}) and then adsorbed on the heterojunctions surface. As H_2 surrounds the heterojunction, H_2 will react with O_{ads} on the CoO surface, causing energy band bending of CoO. However, H_2 hardly reacts with O_{ads} on the SnO_2 surface. This will increase the potential barrier of SnO_2/CoO heterojunctions, thereby increasing the resistance of SnO_2/CoO heterojunctions and generating a p-type response to H_2. In CO

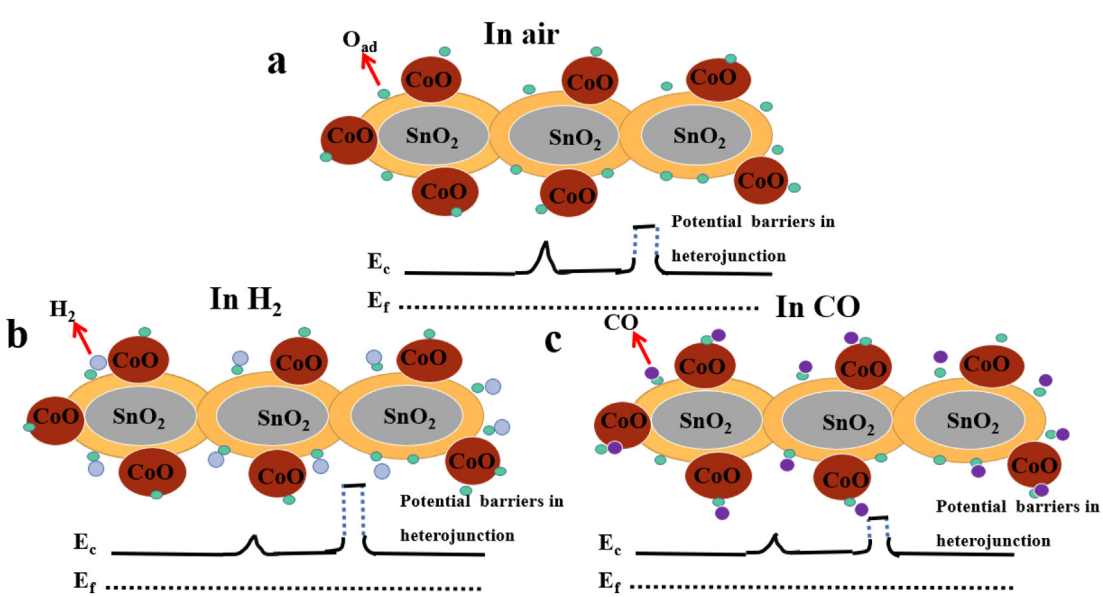

Fig. 11. Gas-sensing mechanism of the CoO/SnO_2 heterojunctions. (a) Air, (b) H_2, and (c) CO.

atmosphere, CO reacts with O_{ads} on both SnO_2 and CoO surfaces of the heterojunctions, and electrons revert to their conduction band. It will reduce heterojunctions' barrier height and resistance. The n-type response to CO for the SnO_2/CoO heterojunction makes an excellent selectivity for H_2 and CO.

4. Conclusion

The first principle was used to study the adsorption performances of H_2 and CO on SnO_2(100)(I)/CoO(110)(II) and CoO(110)(II)/SnO_2(100)(II) nanomaterials surfaces. The adsorption stability of H_2 and CO on the heterojunction surface can be determined according to the adsorption energy and distance. In addition, the d-band center of the heterojunctions approaches the Fermi energy level with the adsorption of O_2, leading to an increased antibonding orbit and decreased probability of the electron occupation. For this reason, H2 and CO can be stably adsorbed on the O2 of the heterojunctions surface. Interestingly, DOS displays that SnO_2(100)(I)/CoO(110)(II) emerges p-type response to H_2, while SnO_2(100)(I)/CoO(110)(II) and CoO(110)(II)/SnO_2(100)(II) display n-type response to CO. As a result, heterojunctions appear an obvious selective response to H_2 and CO. Electron density and electron density difference is used to explain the underlying mechanism of the selectivity in the adsorption performances. The results certificate that exists of electrons and electron conversion between H_2 and O_2 on the SnO_2(100)(I)/CoO(110)(II) surface. Therefore, the potential barrier of SnO_2/CoO heterojunctions increases and shows a p-type response to H_2. Moreover, some electronics and electrons conversion happens between CO and O_2 on SnO_2(100)(I)/CoO(110)(II) and CoO(110)(II)/SnO_2(100)(II) surface. It causes the reduction of heterojunctions potential barrier and displays an n-type response to CO. Thus, SnO_2/CoO nanomaterial achieves a desirable selectivity for H_2 and CO.

Credit author statement

Yunxia He: Investigation, Formal analysis, Data curation, Visualization, Writing-original draft. **Lin Tao**: Conceptualization, Methodology, Resources, Visualization, Writing-review & editing. **Jing Li**: Methodology, Resources, Formal analysis, Validation, Funding acquisition, Project administration. **Mingjie Wu**: Methodology, Formal analysis, Writing-review & editing. **Preeyaporn Poldorn**: Methodology, Formal analysis. **Davoud Dastan**: Methodology, Formal analysis, Writing-review & editing, Conceptualization, Supervision. **Sedigheh Abbasi**: Methodology. **Shuai Nie**: Methodology. **Xitao Yin**: Methodology, Resources, Writing-review & editing. **Qi Wang**: Methodology, Resources, Project administration.

Declaration of competing interest

The authors declare that they have no known competing financial interests or personal relationships that could have appeared to influence the work reported in this paper.

Data availability

No data was used for the research described in the article.

Acknowledgments

The authors are very grateful for the support of the National Natural Science Foundation of China (Grant No. 51974157, 51874169, and 51774180), the Youth Fund of the Education Department of Liaoning Province (LJKQZ20222324), and University of Science and Technology Liaoning Talent Project Grants (601010398) are gratefully acknowledged.

Appendix A. Supplementary data

Supplementary data to this article can be found online at https://doi.org/10.1016/j.mtnano.2023.100334.

References

[1] M. Righettoni, A. Amann, S.E. Pratsinis, Mater. Today 18 (2015) 163–171.
[2] X.-T. Yin, D. Dastan, F. Gity, J. Li, Z. Shi, N.D. Alharbi, Y. Liu, X.-M. Tan, X.-C. Gao, X.-G. Ma, L. Ansari, Sensor Actuator Phys. 354 (2023), 114273.
[3] T.H. Kim, J.W. Yoon, Y.C. Kang, F. Abdel-Hady, A.A. Wazzan, J.H. Lee, Sensor. Actuator. B Chem. 240 (2017) 1049–1057.
[4] T.T. Wang, S.Y. Ma, L. Cheng, J. Luo, X.H. Jiang, W.X. Jin, Sensor. Actuator. B Chem. 216 (2015) 212–220.
[5] D. Dastan, K. shan, A. Jafari, T. Marszalek, M.K.A. Mohammed, L. Tao, Z. Shi, Y. Chen, X.-T. Yin, N.D. Alharbi, F. Gity, S. Asgary, M. Hatamvand, L. Ansari, Mater. Sci. Semicond. Process. 154 (2023), 107232.
[6] L. Tao, D. Dastan, W. Wang, P. Poldorn, X. Meng, M. Wu, H. Zhao, H. Zhang, L. Li, B. An, ACS Appl. Mater. Interfaces 15 (2023) 12534–12544.
[7] C.H. Kwak, H.S. Woo, F. Abdel-Hady, A. Wazzan, J.H. Lee, Sensor. Actuator. B Chem. 223 (2016) 527–534.
[8] L.O. Mark, C. Zhu, J.W. Medlin, H. Heinz, ACS Catal. 10 (2020) 5462–5474.
[9] D.E. Motaung, I. Kortidis, G.H. Mhlongo, M.M. Duvenhage, H.C. Swart, G. Kiriakidis, S.S. Ray, RSC Adv. 6 (2016) 26227–26238.
[10] C.S.L.Q. Kuang, Z. Li, et al., J. Phys. Chem. C 112 (2008) 11539–11544.
[11] A.R. Jayakrishnan, J.P.B. Silva, K. Kamakshi, D. Dastan, V. Annapureddy, M. Pereira, K.C. Sekhar, Prog. Mater. Sci. 132 (2023), 101046.
[12] I. Ashraf, S. Ahmad, D. Dastan, C. Wang, H. Garmestani, M. Iqbal, Electrochim. Acta 442 (2023), 141899.
[13] X.-T. Yin, H. Huang, J.-L. Xie, D. Dastan, J. Li, Y. Liu, X.-M. Tan, X.-C. Gao, W.A. Shah, X.-G. Ma, Green Chem. Lett. Rev. 15 (2022) 546–556.
[14] H.M. Jeong, J.H. Kim, S.Y. Jeong, C.H. Kwak, J.H. Lee, ACS Appl. Mater. Interfaces 8 (2016) 7877–7883.
[15] A. Katoch, Z. Ul Abideen, H.W. Kim, S.S. Kim, ACS Appl. Mater. Interfaces 8 (2016) 2486–2494.
[16] J.H.Y.W.J. Moon, G.M. Choi, Sensor. Actuator. B Chem. 87 (2002) 464–470.
[17] E.C. Davide Barreca, Angelo P. Ferrucci, Alberto Gasparotto, Chiara Maccato, § Cinzia Maragno, Giorgio Sberveglieri, Eugenio Tondello, Chem. Mater. 19 (2007) 5642–5649.
[18] S. Nie, D. Dastan, J. Li, W.D. Zhou, S.S. Wu, Y.W. Zhou, X.T. Yin, J. Phys. Chem. Solid. 150 (2021), 109864.
[19] C.W. Na, H.S. Woo, I.D. Kim, J.H. Lee, Chem. Commun. 47 (2011) 5148–5150.
[20] J.Y. Park, S.-W. Choi, J.-W. Lee, C. Lee, S.S. Kim, J. Am. Ceram. Soc. 92 (2009) 2551–2554.
[21] X.-T. Yin, J. Li, D. Dastan, W.-D. Zhou, H. Garmestani, F.M. Alamgir, Sensor. Actuator. B Chem. 319 (2020), 128330.
[22] D.R. Patil, L.A. Patil, Talanta 77 (2009) 1409–1414.
[23] L. Wang, Y. Kang, Y. Wang, B. Zhu, S. Zhang, W. Huang, S. Wang, Mater Sci Eng C Mater Biol Appl 32 (2012) 2079–2085.
[24] A. Chen, S. Bai, B. Shi, Z. Liu, D. Li, C.C. Liu, Sensor. Actuator. B Chem. 135 (2008) 7–12.
[25] A. Kusior, M. Radecka, M. Rekas, M. Lubecka, K. Zakrzewska, A. Reszka, B.J. Kowalski, Procedia Eng. 47 (2012) 1073–1076.
[26] C. Liangyuan, B. Shouli, Z. Guojun, L. Dianqing, C. Aifan, C.C. Liu, Sensor. Actuator. B Chem. 134 (2008) 360–366.
[27] X.L. Yu, G.J. Zhang, H.B. Cao, X.Q. An, Y. Wang, Z.J. Shu, X.L. An, F. Hua, New J. Chem. 36 (2012) 2593–2598.
[28] Y.J. Liu, G.X. Zhu, J.Z. Chen, H. Xu, X.P. Shen, A.H. Yuan, Appl. Surf. Sci. 265 (2013) 379–384.
[29] I. Ashraf, S. Ahmad, F. Nazir, D. Dastan, Z. Shi, H. Garmestani, M. Iqbal, Int. J. Hydrogen Energy 47 (2022) 27383–27396.
[30] D. Dastan, K. Shan, A. Jafari, F. Gity, X.-T. Yin, Z. Shi, N.D. Alharbi, B.A. Reshi, W. Fu, Ş. Ţălu, L. Aljerf, H. Garmestani, L. Ansari, Appl. Phys. A 128 (2022) 400.
[31] F. Altaf, S. Ahmed, D. Dastan, R. Batool, Z.U. Rehman, Z. Shi, M.U. Hameed, P. Bocchetta, K. Jacob, Mater. Today Chem. 24 (2022), 100843.
[32] H. Gu, Z. Wang, Y. Hu, Sensors 12 (2012) 5517–5550.
[33] W. Wang, Z.Y. Li, W. Zheng, H.M. Huang, C. Wang, J.H. Sun, Sensor. Actuator. B Chem. 143 (2010) 754–758.
[34] M. Rumyantseva, V. Kovalenko, A. Gaskov, E. Makshina, V. Yuschenko, I. Ivanova, A. Ponzoni, G. Faglia, E. Comini, Sensor. Actuator. B Chem. 118 (2006) 208–214.
[35] B.P.J. de Lacy Costello, R.J. Ewen, N.M. Ratcliffe, P.S. Sivanand, Sensor. Actuator. B Chem. 92 (2003) 159–166.
[36] A. Chen, X. Huang, Z. Tong, S. Bai, R. Luo, C.C. Liu, Sensor. Actuator. B Chem. 115 (2006) 316–321.
[37] W.-d. Zhou, D. Dastan, X.-t. Yin, S. Nie, S. Wu, Q. Wang, J. Li, J. Mater. Sci. Mater. Electron. 31 (2020) 18412–18426.
[38] V.B. Kamble, A.M. Umarji, Appl. Phys. Lett. 104 (2014), 251912.
[39] S. Abbasi, D. Dastan, Ş. Ţălu, M.B. Tahir, M. Elias, L. Tao, Z. Li, Int. J. Environ. Anal. Chem. 20 (2022) 1–15.

[40] Y.B. Shen, W. Wang, A.F. Fan, D.Z. Wei, W.G. Liu, C. Han, Y.S. Shen, D. Meng, X.G. San, Int. J. Hydrogen Energy 40 (2015) 15773–15779.
[41] M.K.A. Mohammed, A.K. Al-Mousoi, S. Singh, U. Younis, A. Kumar, D. Dastan, G. Ravi, Energy Fuels 36 (2022) 12192–12200.
[42] Y. Zeng, Y.F. Bing, C. Liu, W.T. Zheng, G.T. Zou, Trans. Nonferrous Metals Soc. China 22 (2012) 2451–2458.
[43] P. Zhu, D. Dastan, L. Liu, L. Wu, Z. Shi, Q.Q. Chu, F. Altaf, M.K.A. Mohammed, J. Mol. Graph. Model. 118 (2023), 108335.
[44] I. Giebelhaus, E. Varechkina, T. Fischer, M. Rumyantseva, V. Ivanov, A. Gaskov, J.R. Morante, J. Arbiol, W. Tyrra, S. Mathur, J. Mater. Chem. 1 (2013) 11261–11268.
[45] T.M. Li, W. Zeng, Z.C. Wang, Sensor. Actuator. B Chem. 221 (2015) 1570–1585.
[46] G.X. Wan, S.Y. Ma, X.W. Sun, A.M. Sun, X.B. Li, J. Luo, W.Q. Li, C.Y. Wang, Mater. Lett. 145 (2015) 48–51.
[47] S. Vallejos, T. Stoycheva, P. Umek, C. Navio, R. Snyders, C. Bittencourt, E. Llobet, C. Blackman, S. Moniz, X. Correig, Chem. Commun. 47 (2011) 565–567.
[48] J.H. Kim, J.H. Lee, A. Mirzaei, H.W. Kim, S.S. Kim, Sensor. Actuator. B Chem. 248 (2017) 500–511.
[49] A. Bonalde, A. Henriquez, M. Manrique,, ISIJ Int. 45 (2005) 1255–1260.
[50] L. Tao, J.C. Huang, D. Dastan, T.Y. Wang, J. Li, X.T. Yin, Q. Wang, Appl. Surf. Sci. 530 (2020), 147265.
[51] L. Tao, J. Huang, D. Dastan, J. Li, X.T. Yin, Q. Wang, Surface. Interfac. 27 (2021), 101462.
[52] W. Lubitz, W. Tumas, Chem. Rev. 107 (2015) 3900–3903.
[53] H. Kim, W. Kim, S. Cho, J. Park, G.Y. Jung, ACS Appl. Mater. Interfaces 12 (2020) 28616–28623.
[54] X.T. Yin, J. Li, Q. Wang, D. Dastan, Z.C. Shi, N. Alharbi, H. Garmestani, X.M. Tan, Y. Liu, X.G. Ma, Langmuir 37 (2021) 13548–13558.
[55] H.-J. Kim, J.-H. Lee, Sensor. Actuator. B Chem. 192 (2014) 607–627.
[56] L. Huo, X. Yang, Z. Liu, X. Tian, T. Qi, X. Wang, K. Yu, J. Sun, M. Fan, Sensor. Actuator. B Chem. 244 (2017) 694–700.
[57] J. Martinez, S.B. Sinnott, S.R. Phillpot, Comput. Mater. Sci. 130 (2017) 249–256.
[58] H. Xiong, Z. Liu, H. Zhang, Z. Du, C. Chen, J. Phys. Chem. Solid. 107 (2017) 162–169.
[59] A. Timoumi, D. Dastan, B. Jamoussi, K. Essalah, O.H. Alsalmi, N. Bouguila, H. Abassi, R. Chakroun, Z. Shi, S. Talu, Molecules 27 (2022) 6151.
[60] P. Poldorn, Y. Wongnongwa, R.-Q. Zhang, S. Nutanong, L. Tao, T. Rungrotmongkol, S. Jungsuttiwong, Int. J. Hydrogen Energy 1 (2023) 360–3199.
[61] L. Wu, S. Li, L. Li, H. Zhang, L. Tao, X. Geng, H. Yang, W. Zhou, C. Sun, D. Ju, B. An, Appl. Catal. B Environ. 324 (2023), 122250.
[62] L. Tao, J.C. Huang, D. Dastan, T.Y. Wang, J. Li, X.T. Yin, Q. Wang, Appl. Surf. Sci. 540 (2021), 148320.
[63] K.B.J.P. Perdew, M. Ernzerhof, Phys. Rev. Lett. 77 (1996) 3865–3868.
[64] L. Tao, J. Huang, D. Dastan, J. Li, X. Yin, Q. Wang, Surface. Interfac. 27 (2021), 101462.
[65] M.J.G.J. Goniakowski, Surf. Sci. 350 (1996) 145–158.
[66] J.R. Kitchin, J.K. Norskov, M.A. Barteau, J.G. Chen, Phys. Rev. Lett. 93 (2004), 156801.
[67] B. Hammer, Top. Catal. 37 (2006) 3–16.
[68] J.K. Norskov, F. Abild-Pedersen, F. Studt, T. Bligaard, Proc. Natl. Acad. Sci. U. S. A. 108 (2011) 937–943.
[69] J.K. Norskov, T. Bligaard, J. Rossmeisl, C.H. Christensen, Nat. Chem. 1 (2009) 37–46.
[70] M. Viitala, O. Cramariuc, B. Delley, T.T. Rantala, Surf. Sci. 605 (2011) 1563–1567.